

Universal scaling in one-dimensional non-reciprocal matter

Shuoguang Liu,^{1,*} Ryo Hanai,² and Peter B. Littlewood^{1,3}

¹*James Franck Institute and Department of Physics, University of Chicago, Chicago IL 60637, USA*

²*Department of Physics, Institute of Science Tokyo,*

2-12-1 Ookayama Meguro-ku, Tokyo, 152-8551, Japan †

³*School of Physics and Astronomy, The University of St Andrews, St Andrews, KY16 9AJ, United Kingdom*

(Dated: March 19, 2025)

Unveiling universal non-equilibrium scaling laws has been a central theme in modern statistical physics, with recent attention increasingly directed toward nonequilibrium phases that exhibit rich dynamical phenomena. A striking example arises in nonreciprocal systems, where asymmetric interactions between components lead to inherently dynamic phases and unconventional criticality near a critical exceptional point (CEP), where the criticality arises from the coalescence of collective modes to the Nambu-Goldstone mode. However, the universal scaling behavior that should emerge in this system with full consideration of many-body effects and stochastic noise remains largely elusive. Here, we establish a dynamical scaling law in a generic one-dimensional stochastic nonreciprocal $O(2)$ -symmetric system. Through large-scale simulations, we uncover a new nonequilibrium scaling in the vicinity of transition, distinct from any previously known equilibrium or nonequilibrium universality classes. In regimes where the system breaks into domains with opposite chirality, we demonstrate that fluctuations are strongly suppressed, leading to a logarithmic scaling as a function of system size L , in contrast to the conventional power-law scaling expected from dynamical scaling theory. This work elucidates the beyond-mean-field dynamics of non-reciprocal matter, thereby shedding light on the exploration of criticality in nonreciprocal phase transition across diverse physical contexts, from active matter and driven quantum systems to biological pattern formation and non-Hermitian physics.

The study of universal scaling laws in nonequilibrium systems has long been one of the central subjects in modern statistical physics. Because the non-equilibrium phases generally violate conditions that must be obeyed in equilibrium, their universal features, such as the scaling exponents, can differ from those observed in equilibrium. In many known nonequilibrium phase transitions, however, the system's non-equilibrium character arises solely from the spatiotemporal noise that breaks detailed balance; without this noise, the properties of the phases and their transitions match those predicted by Landau's theory based on free-energy minimization. Paradigmatic examples of this class include directed percolation [1], Kardar-Parisi-Zhang scaling [2, 3], and flocking [4–8].

In contrast, there exists a class of non-equilibrium phases whose phase transitions cannot be explained solely by the free energy minimization principle—even in the absence of noise. For example, the Belousov-Zhabotinsky reaction [9, 10] exhibits a time-dependent limit cycle phase [11–14]. Because continuous injection of energy is necessary to sustain this dynamic state, the system displays a non-equilibrium characteristic even at a mean-field level. As a result, these dynamical phases lack a static free-energy description.

Recently, a novel type of nonequilibrium phase transition of the latter, non-reciprocal phase transition [15–19], has gained attention. In non-equilibrium systems that break the detailed balance condition, the coupling between the variables can be non-reciprocal [20–25]. As a result, the system may exhibit a non-equilibrium phase transition to a phase where the macroscopic quantities

display persistent time-dependent many-body chase-and-runaway dynamics [15–17, 23, 26, 27]. Uniquely, the transition point is characterized by the emergence of a critical exceptional point (CEP) [19, 28] — a point where a collective mode coalesces with the Nambu-Goldstone mode.

A variety of systems in very different contexts are shown to exhibit CEPs: they range from classical active systems such as a multi-species non-reciprocal matter [15, 29], non-reciprocal pattern formation [16, 17, 22], to quantum systems such as driven-dissipative condensates [18, 30], ferrimagnets [31], layered ferromagnets [32], and collective spin dynamics [27, 33]. CEP exhibits exotic features with no equilibrium counterparts, such as anomalously enhanced fluctuations [19, 34], diverging entropy production [35–37], and fluctuation-induced first-order transition [28]. However, to our knowledge, no existing work has studied the universal scaling behaviors near CEP that *fully* incorporates nonlinear many-body effects and stochastic noise in a spatially extended system.

In this paper, we establish a dynamical scaling law that arises in a generic one-dimensional nonreciprocal $O(2)$ model, which is a paradigmatic model exhibiting CEPs, by a direct large-scale numerical simulation. Figure 1(a) summarizes our key findings. In the absence of noise $\sigma = 0$, there is a distinct phase transition between a dynamic chiral phase and a static phase, which is characterized by the CEP. These phases become disordered once the noise is introduced $\sigma > 0$, and the transition between the two regimes becomes a crossover, giving rise to a critical region (in a similar manner to a quantum

critical point). While in the static disordered regime, we observe simple diffusion dynamics, the fluctuations are anomalously enhanced in the vicinity of the CEP [19]. We show that the scaling relationship is very different from any known universal scaling, which we expect is a new nonequilibrium universality class.

Surprisingly, in the region where the system break into domains with opposite chirality (which we call the 'chiral disordered regime' in this paper), we find that the scaling relation transits to a regime where the fluctuation is strongly suppressed. We demonstrate that fluctuations in this regime scale *logarithmically* as a function of system size $\sim 2\gamma \log L$ (in contrast to the conventional algebraic scaling $\sim L^{2\alpha}$, where L is the system size), similarly to what is observed in a quasi-long-range order. We note that this type of logarithmic non-equilibrium scaling law has also been observed numerically at the critical point of a one-dimensional rough surface growth with evaporation at the edges of plateaus [1, 38]. We have strong evidence that the phenomenon we observed here is attributed to the dynamical origins of the chiral phase and the occurrence of a spatiotemporal topological vortex that necessarily arises when domains with opposite chirality are present.

MODEL

We consider fluctuating hydrodynamics of a non-reciprocally interacting two-species ($a = A, B$) order parameter, which is governed by the equation of motion

$$\partial_t \vec{P}_a = \alpha_{ab} \vec{P}_b + \beta_{abcd} (\vec{P}_b \cdot \vec{P}_c) \vec{P}_d + D_{ab} \partial_x^2 \vec{P}_b + \vec{\xi}_a. \quad (1)$$

where the repeated index implies summation. Here, $\vec{P}_a(x, t) = (P_a^x(x, t), P_a^y(x, t)) = |P_a|(\cos \theta_a, \sin \theta_a)$ is an order parameter that characterizes the $O(2)$ symmetry breaking and α_{ab} and β_{abcd} are real coefficients that are crucially allowed to be asymmetric (e.g. $\alpha_{ab} \neq \alpha_{ba}$), reflecting the non-equilibrium nature of the system. D_{ab} is the (cross) diffusion constant and $\vec{\xi}_a(x, t) = (\xi_a^x(x, t), \xi_a^y(x, t))$ is a Gaussian white noise satisfying $\langle \xi_a^i(x, t) \rangle = 0$ and $\langle \xi_a^i(x, t) \xi_b^j(x', t') \rangle = \sigma \delta_{ab} \delta_{ij} \delta(x - x') \delta(t - t')$, ($i, j = x, y$).

To be concrete, in the following sections, we set the coefficients $\alpha_{ab}, \beta_{abcd}, D_{ab}$ such that

$$\partial_t \mathbf{P}(x, t) = \hat{A}(\partial_x) \mathbf{P}(x, t) + \boldsymbol{\xi}(x, t), \quad (2)$$

where $\mathbf{P} = (\vec{P}_A, \vec{P}_B)^T$, $\boldsymbol{\xi} = (\vec{\xi}_A, \vec{\xi}_B)^T$,

$$\hat{A}(\partial_x) = \begin{pmatrix} j_{AA} - \|\vec{Q}_A\|^2 + D_A \partial_x^2 & j_{AB} \\ j_{BA} & j_{BB} - \|\vec{Q}_B\|^2 + D_B \partial_x^2 \end{pmatrix}$$

and $\vec{Q}_A = j_{AA} \vec{P}_A + j_{AB} \vec{P}_B$, $\vec{Q}_B = j_{BB} \vec{P}_B + j_{BA} \vec{P}_A$. This choice corresponds to the coarse-grained description of a non-reciprocal XY model as depicted in Fig. 1(b). In

this model, the spins on different sublattice A and B are coupled in an asymmetric manner ($j_{AB} \neq j_{BA}$), while the coupling between the same sublattice are ferromagnetic $j_{AA}, j_{BB} > 0$.

As mentioned earlier, in the absence of noise, the non-reciprocal coupling $j_{AB} \neq j_{BA}$ gives rise to two distinct phases [15]. (See Fig. 1(a).) When the coupling is reciprocal (i.e., $j_{AB} = j_{BA}$), the system always converges to a static phase where A and B remain aligned or anti-aligned by spontaneous breaking of $U(1) \subset O(2)$ symmetry. When a non-reciprocity is introduced, on the other hand, the system may exhibit a non-reciprocal phase transition to a dynamical chiral phase, where A and B rotate at a constant angular speed $\dot{\theta}_a = \Omega_a (\neq 0)$ while maintaining a fixed relative angle, either clockwise (right-handed) or counterclockwise (left-handed) and hence spontaneously breaks the $\mathbb{Z}_2 \subset O(2)$ symmetry. Notably, the static-chiral phase boundary is marked by CEPs, where the transition occurs through the coalescence of the collective damped mode Goldstone mode arising from the spontaneous $U(1)$ symmetry-breaking (Fig. 1(c)).

Below, we address how a stochastic noise $\sigma > 0$ and spatial gradient D_a affects these phases and phase transitions (See Methods for details.) Since our system is one-dimensional, an infinitesimally small noise destroys the order, i.e., $\langle \vec{P}_a \rangle = 0$. However, we will see that the interplay between the nonreciprocity-driven dynamics and a beyond-mean-field effect gives rise to novel non-equilibrium scaling properties in their fluctuation properties.

DYNAMICAL SCALING HYPOTHESIS

To quantitatively study spatiotemporal fluctuations and their unique nonequilibrium scaling behavior in the vicinity of CEPs, we analyze the time correlation function of the order parameter

$$C_{aa}(t_0, t_0 + t; L) = \left\langle \frac{\overline{\vec{P}_a(t_0 + t, x) \cdot \vec{P}_a(t_0, x)}}{|\overline{\vec{P}_a(t_0, x)}|^2} \right\rangle \quad (3)$$

where $a = A, B$ labels the species, $\overline{(\dots)} = \frac{1}{L} \int_x (\dots)$ is the spatial average over the system of size L , and $\langle \dots \rangle$ is the ensemble average over different stochastic trajectories. In the regime where stochastic noise is not too strong such that $\langle |\vec{P}_a| \rangle \neq 0$ (while $\langle \vec{P}_a \rangle = 0$ when the system is in the disordered phase), amplitude fluctuations are generically overdamped and phase fluctuations are dominant. In this case, the relationship between the correlation functions can be approximated as [39]

$$-\log |C_{aa}(t_0, t_0 + t; L)| \simeq \frac{1}{2} \text{Var}[\theta_a(x, t_0 + t) - \theta_a(x, t_0)] \quad (4)$$

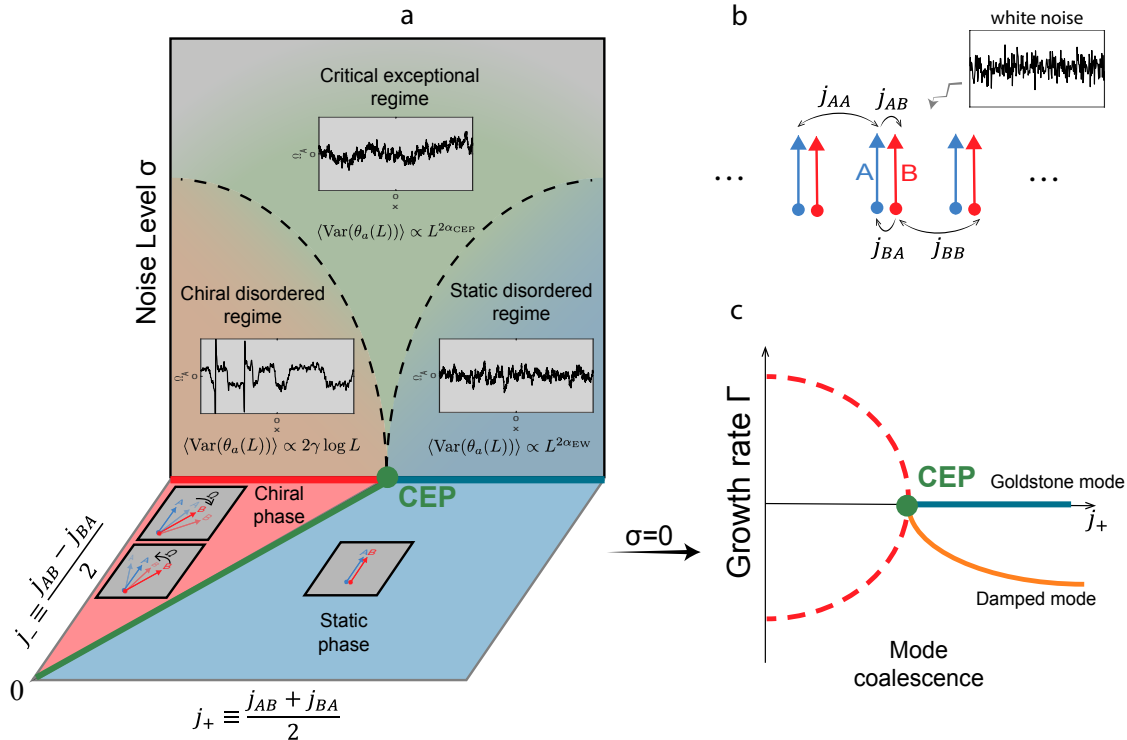


FIG. 1. **Stochastic non-reciprocal $O(2)$ model and the schematic phase diagram.** (a) Schematic phase diagram of non-reciprocal $O(2)$ symmetric model. In the absence of noise, the phase boundary (green line) marked by critical exceptional points (CEPs) separates the chiral and static phases. At finite noise, these phases become disordered, and a critical regime that exhibits a nonequilibrium scaling relation emerges in the vicinity of the CEP. Insets in the three disordered regimes: Spatial profiles of the frequency $\Omega_A(x)$ after long-time evolution and distinct scaling relations of the phase correlation. $\Omega_A(x)$ in the critical exceptional regime exhibits more pronounced fluctuations compared to the static regime, while in the chiral disordered regime, dynamical oscillations arise at the boundary between domain walls. Whereas the phase correlations in the critical and static regimes follow power-law scaling with system size (but with different critical exponents), those in the chiral regime obey a logarithmic scaling. (b) The non-reciprocal XY model, a microscopic example that coarse-grains to Eq. (1). This model describes a noisy 1D chain of two species of agents coupled non-reciprocally ($j_{AB} \neq j_{BA}$). The intra-species couplings are represented by j_{AA} and j_{BB} . Each agent has only one degree of freedom—rotation, obeying $O(2)$ symmetry. (c) Schematic diagram of the transition between static and chiral phases through the coalescence of a damped mode (solid orange) and a Goldstone mode (solid blue) at a CEP (green circle). Note that the growth rate ($\Gamma \equiv \pm i\Omega$) of the left-/right-handed chiral modes (dashed red) is imaginary.

which quantifies the magnitude of phase fluctuations.

To obtain a nonequilibrium universal relation in our model, we adopt the dynamic scaling hypothesis, which states that the correlation functions follow the Family-Viscek scaling relation:

$$-\log |C_{aa}(t_0, t_0 + t; L)| = |L|^{2\alpha} \mathcal{F}\left(\frac{t}{|L|^z}\right) \propto L^{2\alpha}, t \rightarrow \infty \quad (5)$$

where $\mathcal{F}(x)$ a scaling relation, α is the roughness exponent and z is the dynamical exponent.

Since the two species A and B are coupled, they share a common asymptotic behavior, which we have confirmed numerically (See SI.). Therefore, it is enough to focus on one of the components (C_{AA}), as is done below.

NONEQUILIBRIUM SCALING AT CEP

Fig. 2(a) shows the time correlation function $-\log |C_{AA}(t_0, t_0 + t; L = 2^{12})|$ as a function of j_+ at small but finite noise strength $\sigma = 0.005$ (with fixed non-reciprocity j_-). Here, we set large t and t_0 such that the correlation function converges. Notably, fluctuation is enhanced by a few orders of magnitudes in the vicinity of the CEP $j_+ \sim 0.0097$. This implies the emergence of anomalously enhanced phase fluctuations arising from CEP.

To quantify this point in more detail, we examined the system size dependence and the time evolution of the correlation function near and far from the CEP for different system sizes L , as shown in Figs. 2(b). When

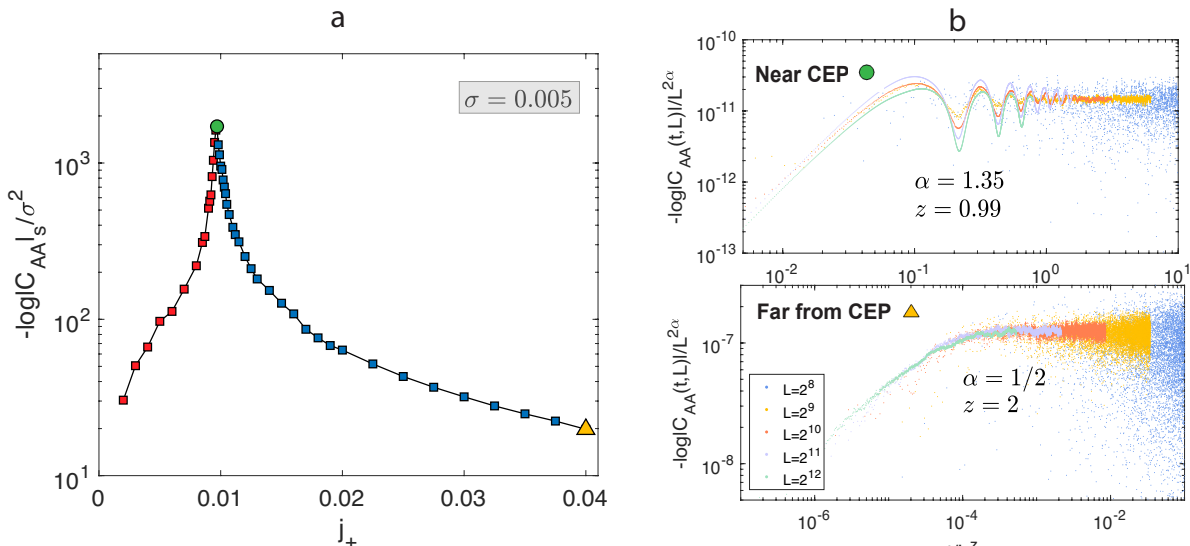


FIG. 2. **Critical fluctuation and scalings near/far from the CEP.** (a) Fluctuation across j_+ axis at low noise. The fluctuation peaks at the CEP (green circle $j_+ = 0.0097$), and flattens out when far from the CEP (yellow triangle $j_+ = 0.0400$). The rates of change of the fluctuation differs between the chiral disordered regime (left, red square) and the static disordered regime (right, blue square). The fluctuation at each j_+ is measured as the time average of the correlation function $-\log|C_{AA}(t, L)|$ (as in Eq. 3) after a certain saturation time. The system size is $L = 2^{12}$. (b) Finite-size scaling collapse of $-\log|C_{AA}(t, L)|$ at the CEP (upper panel) with $\alpha = 1.35, z = 0.99$, which we hypothesize is a new universality class. By contrast, the Edwards-Wilkinson (EW) far from the CEP (lower panel) follows $\alpha = 1/2, z = 2$. In (b), the upper panel corresponds to $j_+ = 0.0097$, and the lower panel to $j_+ = 0.0400$. All correlation functions above are computed by numerically evolving dynamical equations Eq. (2) from the initial uniform steady states, then averaging over 240 realizations. To ensure the convergence of all $-\log|C_{AA}(L)|$, the waiting times are set to $t_0 = 7000$ near the CEP and $t_0 = 1000$ for correlations far from CEP, respectively. A longer convergence time is needed at CEP due to the occurrence of critical slowing down. For all panels, the noise strength is $\sigma = 0.005$, and the diffusion constants are set at $D_A = 100, D_B = 1$, ensuring that no dynamical pattern formation occurs. Other parameters are fixed at $j_- = -0.25$ and $j_{AA} = j_{BB} = 0.5$ across all figures. Panel (b) is plotted in log-log scale, and Panel (a) is in semi-logarithmic scale.

the system is far from the CEP (lower panel), we find a scaling collapse consistent with Eq. (5) by setting the scaling exponents to the Edward-Wilkinson (EW) scaling $\alpha_{EW} = 1/2, z_{EW} = 2$. This implies that the dynamics of the phases are simple diffusion, which can be readily understood as follows. In this regime, among the two modes arising from the two phases $\theta_A(x, t)$ and $\theta_B(x, t)$, one of the modes, which is a relaxation mode, is gapped away through coarse-graining and plays no role in the effective low-energy physics ($k \rightarrow 0$). As a result, the remaining diffusive Goldstone mode (which is an in-phase mode characterized by the dynamics of the center-of-mass phase $\Theta(x, t) = (\theta_A(x, t) + \theta_B(x, t))/2$) governs the dynamics. This diffusive dynamics, constrained by the $O(2)$ symmetry, can be shown to belong to the EW universality class (See Methods).

The upper panel in Fig. 2(b) demonstrates that the behavior near the CEP is significantly different from this simple diffusion. The first remarkable feature is the anomalously large roughening exponent, which is found to be $\alpha_{CEP} = 1.35(5)$. The extracted exponent $\alpha_{CEP} = 1.35(5)$ is to be compared to the roughening ex-

ponent in the EW and KPZ scaling $\alpha_{EW} = \alpha_{KPZ} = 0.5$, implying the occurrence of the anomalously enhanced phase fluctuations in the vicinity of CEPs. As a sanity check, we also computed the quantity (for $a = A$ component) that is routinely used to measure the width of a rough surface,

$$w_a(t, L) = \overline{\langle (\theta_a(x, t) - \bar{\theta}_a(x, t))^2 \rangle} \quad (6)$$

by unwinding the phase from $[-\pi, \pi)$ to $(-\infty, +\infty)$, and obtained a consistent result (Fig. 3(a)). This confirms that phase fluctuations in this regime dominate the fluctuations.

Such an anomalous phase fluctuation at the CEP has been predicted to arise *within a linearized theory* [19], where the roughening exponent was predicted to be $\alpha_{Gauss} = 3/2$ (See Methods). The anomalous enhancement of fluctuations can be understood intuitively as follows. As one approaches the CEP, the damped relaxational mode coalesces with the existing Goldstone mode. This coalescence converts all the noise-activated fluctuation to the Goldstone mode, leading to giant phase fluctuations causing anomalous scaling. The exponent

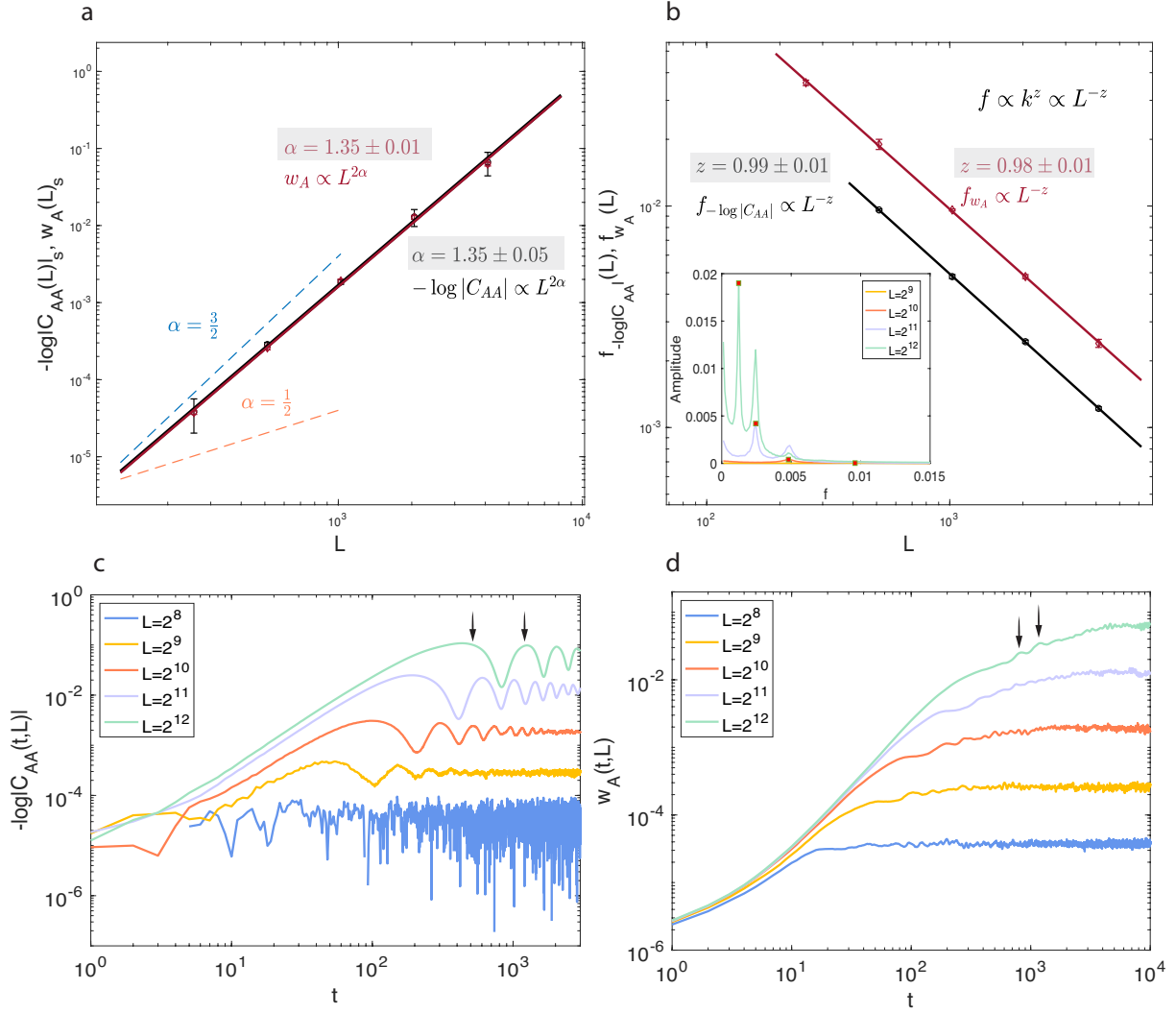


FIG. 3. **Finite size scalings near CEP.** (a) Extraction of the roughness exponent α from the averaged correlations in the saturated region. $-\log|C_{AA}(L)|$ and $w_A(L)$ both scale with $L^{2\alpha}$ with $\alpha = 1.35 \pm 0.05$ (black) and $\alpha = 1.35 \pm 0.01$ (red) respectively. $\alpha = 3/2$ (dash blue) for the Gaussian scaling near CEP and $\alpha = 1/2$ (dash orange) for the EW scaling far from CEP are plotted as the guide for the eyes. The waiting time is set to $t_0 = 7000$ (same choice for Panel (c)). (b) Fit of the dynamical exponent z from the fundamental frequencies $f_{-\log|C_{AA}|}$ (or f_{w_A}) of $-\log|C_{AA}(L)|$ (or $w_A(L)$). Both scale with L^{-z} perfectly for $z = 0.99 \pm 0.01$ (black) and $z = 0.98 \pm 0.01$ (red) respectively, which imply the dynamic of sound modes ($z = 1$). Inset: The amplitude spectra of $-\log|C_{AA}(L)|$ in the frequency domain at various system size. The red squares mark the peak positions of the fundamental frequencies. (c) Behavior of the full correlation $-\log|C_{AA}(t,L)|$ as a function of time in the systems of sizes $L = 2^8 - 2^{12}$. The gapless oscillatory sound modes can be clearly identified (black arrows), which is unique to CEP. (d) Behavior of the phase-phase correlation $w(t,L)$ as a function of time. Periodic sound modes again show up (black arrows). For all panels, the initial conditions are the uniform steady states, and the ensemble size is 240 realizations. The parameters are fixed at $\sigma = 0.005$, $j_+ = 0.0097$, $j_- = -0.25$, $D_A = 100$, $D_B = 1$, $j_{AA} = j_{BB} = 0.5$ across all panels. All panels are in log-log scale.

$\alpha_{\text{CEP}} = 1.35(5)$ that we determined is close to, but not identical to $\alpha_{\text{Gauss}} = 3/2$, which we attribute to nonlinear many-body effects. This picture is consistent with the fact that the width of $\Delta\theta(x,t) = \theta_A(x,t) - \theta_B(x,t)$ is small compared to that of $\Theta(x,t) = (\theta_A(x,t) + \theta_B(x,t))/2$ (See SI).

Another key distinction in the correlations at the CEP is the presence of periodic oscillations of fluctuations,

which is clearly seen in the Fourier-transformed amplitude spectra (inset in Fig. 3(b) and SI.) of the time evolution of C_{AA} and $w_a(t,L)$ (Fig. 3(c) and (d)). This implies the emergence of a sound mode that gives rise to a standing wave with a wavelength $\lambda \sim L$ and frequency f that scale as $f \propto L^{-z}$ with a ballistic dynamical exponent $z = 0.99(1) \approx 1$. This picture is consistent with the linearized theory, which also predicts the emergence

of sound modes [19, 28]. Interestingly, our numerics suggest that this is unaffected by the nonlinear many-body effects (up to our numerical accuracy).

We note that, in the early stage of Fig. 2(b), although the periodic oscillation peaks align well when rescaled with $z = 0.99(1)$, the oscillation amplitudes do not collapse perfectly. This discrepancy arises from the fact that the eigenmodes at the CEP are inherently complex, comprising *both* a sound component and a diffusive component, which evolve on different timescales that scale differently with system size L (See SI). Coherent dynamics dominate the early growth stage, while diffusive dynamics take over in the late saturation stage, gradually damping the oscillations. As a result, no single dynamical exponent z can achieve a perfect collapse [28], which is yet another characteristic of CEP physics. (See more discussion in SI.)

STRONG SUPPRESSION OF FLUCTUATION AND SPATIOTEMPORAL VORTICES

So far, we have implicitly assumed that a uniform state is stable against perturbations. However, in nonequilibrium systems like ours, it is quite common to see instabilities toward pattern formation. Indeed, as shown in Fig. 4(a) and SI Movie, a pattern-forming instability takes place when the ratio of diffusion constants between the different species D_A/D_B is tuned.

Remarkably, we find that fluctuation is strongly suppressed when such pattern formation takes place. Fig. 4(b) shows the correlation function $-\log |C_{AA}(t_0 + t, t_0; L)|$ in this regime at late times as a function of system size L , when finite noise is added $\sigma = 0.1$ (black line). We find the scaling $-\log |C_{AA}(t_0 + t, t_0; L)| \sim 2\gamma \log L$ with $\gamma = 0.25(1)$. This is in stark contrast to the power law seen in EW or CEP scaling $-\log |C_{AA}(t_0 + t, t_0; L)| \sim L^{2\alpha}$ (See Fig. 4(c). Note that panel (c) is plotted with a log-log scale, while panel (b) is plotted with a semi-log scale.) Surprisingly, the presence of noise is irrelevant for such logarithmic scaling to appear, where we find that $-\log |C_{aa}(L)|$ follows the same logarithmic scaling with almost the same exponent even in the absence of noise $\sigma = 0$ (red line). In this case, fluctuation seems to arise because the system is not commensurate with the length of the dynamical pattern, making the system keep on “wiggling” around a well-defined pattern (See SI. and SI Movie).

Interestingly, the fluctuation of the difference between the phases $\Delta\theta(x, t) = \theta_A(x, t) - \theta_B(x, t)$ obeys the same scaling as those of $\theta_A(x, t)$ or $\theta_B(x, t)$ (orange line). This is in stark contrast to the static disordered regime and the CEP regime, where the fluctuation is dominated by the Goldstone mode associated with the global $U(1)$ symmetry breaking, which is governed by the center of mass phase fluctuations $\Theta(x, t) = (\theta_A(x, t) + \theta_B(x, t))/2$.

We note that C_{aa} is still dominated by phase fluctuations in this regime, where we have checked that amplitude fluctuation only gives a subdominant effect $\text{Var}(|\vec{P}_a(x, t)|)(L) \sim \text{const.}$ (See SI.).

We currently do not have a simple explanation of why a strong suppression of phase fluctuation with logarithmic scaling arises. However, we have strong numerical evidence that this is due to the occurrence of spatiotemporal vortices. As shown in Fig. 5(a), (for the case where noise is absent $\sigma = 0$), a spatiotemporal vortex lattice appears in the regimes where logarithmic scaling occurs. There, the amplitude vanishes ($|\vec{P}_a(x_*, t_*)| = 0$) at the position of the defects (x_*, t_*) and the phase difference $\Delta\theta(x, t)$ has a non-trivial winding number $w = \oint_C (dt, dx) \cdot (\partial_t, \partial_x) \Delta\theta(x, t) = \pm 1$ for the contour of the integral C that winds around the defect in the position-time space (x_*, t_*) . These spatiotemporal vortices form a lattice in both space and time directions, splitting the system into domains of different chirality. Since the topological defects split the system into domains with opposite chirality (See inset in Fig. 5(a)), we will call this regime a ‘chiral disordered regime’ below.

We note that the spatiotemporal topological lattice is expected to induce a Goldstone mode associated with the spontaneous breaking of translational invariance (i.e., phason modes), which is different from those arising from a global $U(1)$ symmetry breaking. In contrast to the latter that gives rise to large fluctuations for the center of mass phase $\Theta(x, t)$, the phason modes may induce large fluctuations to the phase difference $\Delta\theta(x, t)$ as well, which may explain why $\text{Var}\Delta\theta(x, t)$ dominates the low energy physics in this regime. We speculate that there might be a mechanism in which the spacetime (1+1D) lattice associated with phason modes might give a similar scaling, which remains an open question for future work.

Interestingly, this chiral disordered regime with strong suppression of fluctuation can appear even in regimes where dynamical instability does *not* take place in the deterministic limit, by adding a strong enough noise (green line). Figure 5(b) shows the correlation function $-\log |C_{aa}|$ as a function of noise strength σ in the vicinity of CEP. While for weak enough noise $\sigma \lesssim 0.02$, the system obeys a CEP scaling $L^{2\alpha}$ with $\alpha = 1.35$, the scaling crosses over to the logarithmic scaling $-\log |C_{aa}| \sim 2\gamma \log L$ when the noise exceeds a certain value $\sigma \gtrsim 0.03$. In the latter regime, noise induces spatiotemporal vortices that split the system into domains (in a similar manner occurring to one-dimensional Ising model) with different chirality, analogously to those occurring due to dynamical instability (See SI.). This implies that these regimes (noise-induced and dynamical instability-induced chiral disordered regimes) may be identified as the same phase of matter.

The phase diagram presented in Fig. 5(c) demonstrates that the noise enhances the chiral disordered regime

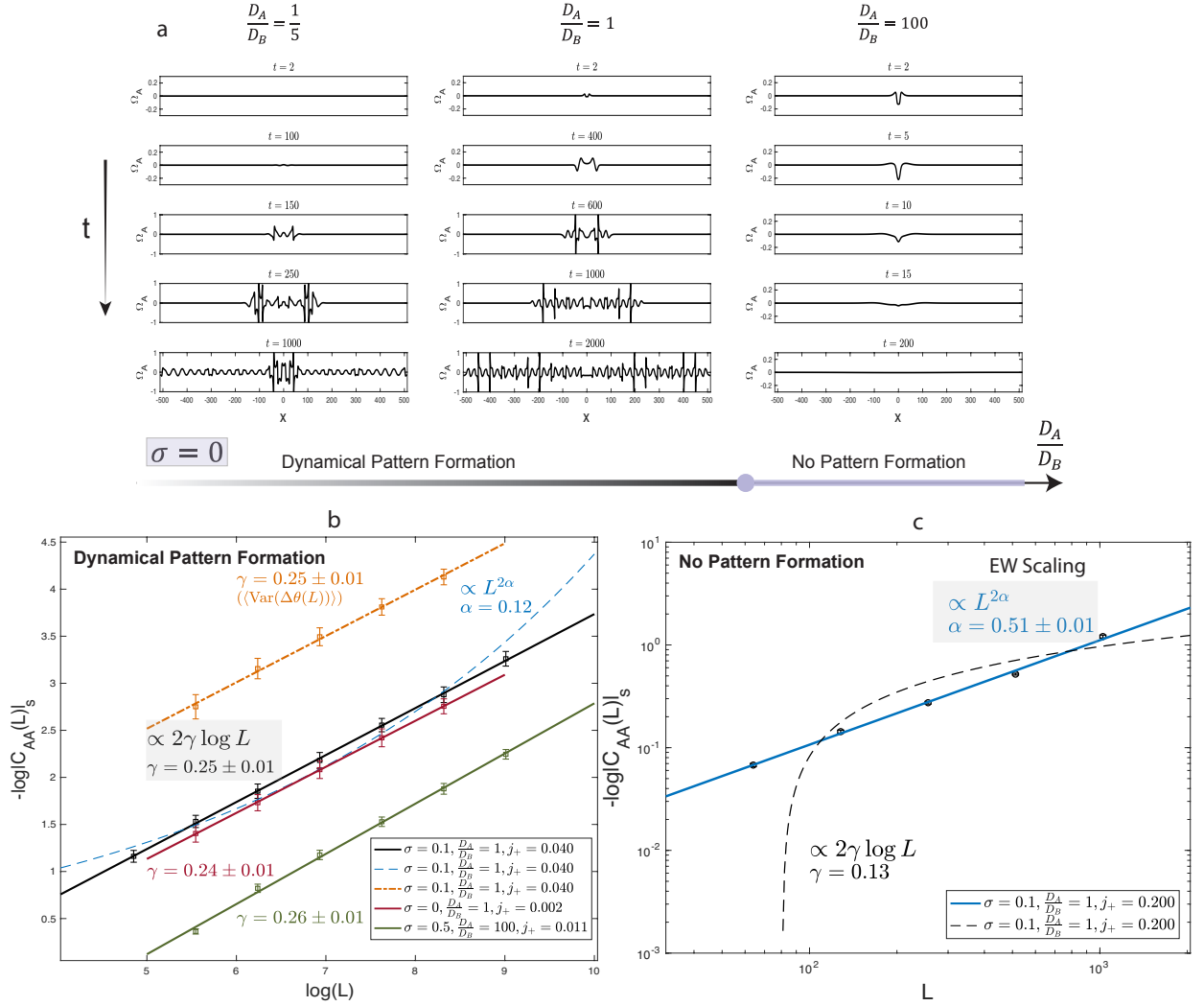


FIG. 4. **Development of the dynamical pattern in the chiral disordered regime** (a) Effect of the diffusion ratio D_A/D_B on the time evolution of $\Omega_A(x, t)$ at zero noise ($\sigma = 0$). The system starts from a uniform steady state with a small Gaussian wave-packet perturbation. When D_A/D_B is large enough, the perturbation damps out, but for comparable D_A and D_B , it triggers a persistent dynamical pattern across the system. In the $D_A/D_B = 1/5$ case, the initial perturbation amplitude is 10^3 times smaller than that in the other two cases, yet still initiates pattern formation, indicating that a smaller D_A/D_B enhances instability (See SI Movie). To reveal the full pattern structure, the Ω -scale is enlarged to $(-1, 1)$ at late times in the left and middle panels. (b) Finite-size scalings in the chiral disordered regime. In the deterministic pattern formation regime ($D_A/D_B = 1$), a logarithmic scaling spanning $L = 2^7 - 2^{13}$ (black line) is identified, with a critical exponent $\gamma = 0.25 \pm 0.01$ in $-\log|C(L)|_s \propto 2\gamma \log L$ (a power-law fit in blue dashed line is included for comparison); in the absence of noise (red line), the logarithmic scaling persists, with $\gamma = 0.24 \pm 0.01$. In the noise-driven pattern formation regime ($D_A/D_B = 100$), the same logarithmic scaling with $\gamma = 0.24 \pm 0.01$ again arise (green line). We also verify that $\text{Var}(\Delta\theta(L))$ where phase difference $\Delta\theta = \theta_A - \theta_B$, follows a similar scaling law with $\gamma = 0.25 \pm 0.01$. Other parameters in $C_{AA}(t_0 + t, t_0; L)$ are: $t_0 = 800, t = 1200$ for all system sizes. (c) Finite-size scaling in the static disordered regime. A power-law scaling spanning $L = 2^6 - 2^{10}$ (blue line) is identified, with $\alpha = 0.51 \pm 0.01$ in $-\log|C(L)|_s \propto L^{2\alpha}$, consistent with EW scaling. We set $j_+ = 0.200$ in this panel. Other parameters in $C_{AA}(t_0 + t, t_0; L)$ are: $t_0 = 10000, t = 40000$ for $L = 2^6 - 2^9$, and $t_0 = 10000, t = 90000$ for $L = 2^{10}$. Notice that (c) is in semi-logarithmic scale on the x-axis, while (d) is in log-log scale. For all panels, $j_- = -0.25$ and $j_{AA} = j_{BB} = 0.5$.

that exhibits logarithmic scaling. Here, we have determined the phases by numerically extracting β with $-\log|C_{aa}(t_0, t_0 + t; L)| \sim t^{2\beta}$. Since we know that the EW scaling arising in the static disordered regime is given by $\beta_{EW} = 1/4$, the deviation from this value signals the departure from the static disordered regime. (Note that

β cannot be extracted in the chiral disordered regime due to the presence of dynamical oscillations, even in the early growth stage.)

Finally, we argue below the scenario on why the spatiotemporal lattice is formed in the presence of dynamical instability. For simplicity, let us consider the case

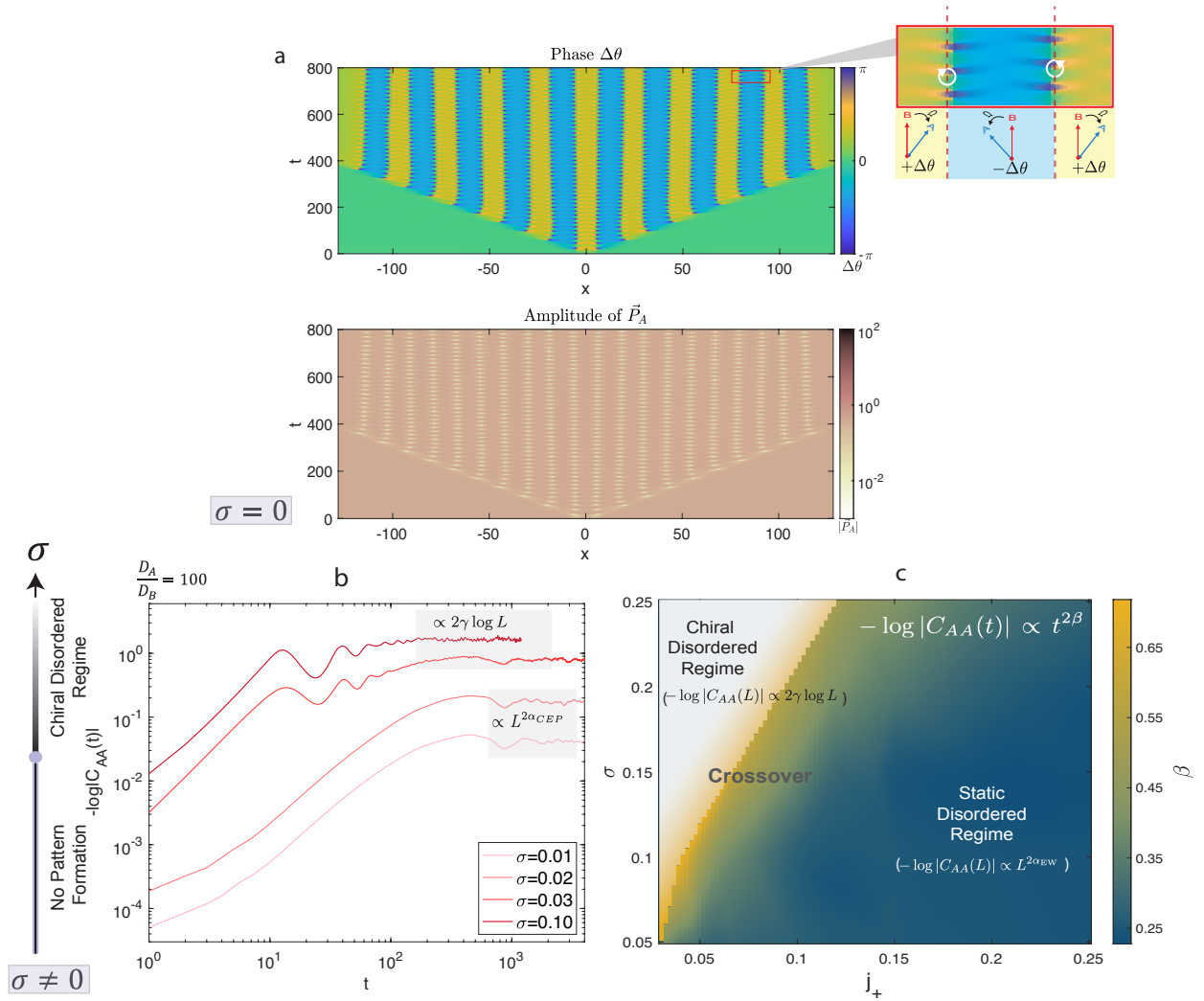


FIG. 5. **Noise-induced logarithmic scaling regime with spatiotemporal vortices.** (a) Time evolution of the phase difference and amplitude from a small perturbation. The spatiotemporal points of topological defects, where $|\vec{P}_A(x_*, t_*)| = 0$ in the amplitude profile, precisely coincide with those where the phase difference $\Delta\theta(x_*, t_*) = 0$. Inset in the upper panel: a zoom-in view of the domains with opposite chirality $+\Delta\theta$ ($-\Delta\theta$) and a (anti-)vortex (\odot) (\ominus) around $\Delta\theta(x_*, t_*) = 0$. The parameters are set at $L = 2^8$, $D_A/D_B = 1$ and $j_+ = 0.011$. (b) Effect of stochastic noise strength σ on $-\log|C_{AA}(t_0 + t, t_0; L)|$. For $\sigma \lesssim 0.02$, no pattern forms, and the correlation behaves similarly to CEP scaling in Fig. 3(d). For $\sigma \gtrsim 0.03$, the emerged dynamical pattern leads to fast oscillations in the correlation and significantly altering its overall growth behavior. The parameters are set at $L = 2^{12}$, $t_0 = 1000$, and $j_+ = 0.011$. (c) $\sigma - j_+$ phase diagram overlaid with a color map for the growth exponent β in $-\log|C_{AA}(t)| \propto t^{2\beta}$. The system size is $L = 2^{12}$. Since EW scaling arising in the static disordered regime is given by $\beta_{EW} = 1/4$, the deviation from this value signals the departure from this regime. The chiral disordered regime is marked in white because β cannot be extracted in the presence of dynamical oscillations. For all panels, $j_- = -0.25$ and $j_{AA} = j_{BB} = 0.5$.

where the system is in the chiral phase when the spatial gradients $O(\partial_x)$ and the noise σ are turned off. Let us further assume that this uniform chiral state is dynamically unstable when the diffusion terms are turned back on. In such a situation, recalling that the chiral phase is characterized by the oscillation of the phases with frequency $\Omega_a = \dot{\theta}_a$ that spontaneously breaks the \mathbb{Z}_2 symmetry, the dynamical instability is expected to make the oscillation frequency vary spatially (often periodic in space), i.e., $\langle \Omega_a(x) \rangle_t (= \langle \Omega_a(x + \ell) \rangle_t)$, where

the $\langle (\dots) \rangle_t$ is the time average over long enough time and ℓ is the length of the pattern. However, such spatial variance of $\langle \Omega_a(x) \rangle_t$ would necessarily cause singularity, which is seen as follows. The time dependence of the phase with spatially varying $\langle \Omega_a(x) \rangle_t$ gives $\theta_a(x, t) \approx \theta_a(x, t=0) + \langle \Omega_a(x) \rangle_t t$ at long times. Assuming that $\langle \Omega_a(x) \rangle_t$ is a smooth function of x , the gradient of the phase grows without a bound, $d\theta_a(x, t)/dx \approx d\theta_a(x, t=0)/dx + (d\langle \Omega_a(x) \rangle_t/dx)t$, which is unphysical. This implies that the time-averaged frequency cannot be

spatially dependent $\langle \Omega_a(x) \rangle_t = \Omega_a^0$, unless the regions are separated by singular points. As the dynamical instability in the system does not support a uniform state, this argument implies that spatiotemporal vortices separate the system into small domains with opposite chirality (i.e., $\langle \Omega_a(x) \rangle_t = \Omega_a^0$ in one domain but $\langle \Omega_a(x) \rangle_t = -\Omega_a^0$ in the other, as seen in Fig. 5(a) and the inset in the chiral disordered regime in Fig. 1(a).

CONCLUSION AND OUTLOOK

In conclusion, we have established a dynamical scaling law in a one-dimensional nonreciprocal $O(2)$ model, revealing a distinct nonequilibrium scaling near the CEP beyond linearized theory. We also demonstrate that in the chiral disordered regime where dynamical pattern formation emerges, fluctuations are strongly suppressed, leading to logarithmic scaling rather than the conventional power-law behavior predicted by dynamical scaling theory. These findings highlight the fundamentally different nature of criticality in nonreciprocal systems compared to equilibrium and previously known nonequilibrium universality classes.

Looking ahead, our results open several avenues for further exploration. A key question is whether similar scaling behavior extends to higher-dimensional nonreciprocal systems and other symmetry classes. We expect these insights could be tested experimentally in active matter [15–17, 22, 40, 41] or driven quantum systems [18, 25, 27, 28, 31–33], where CEP emerge. More broadly, our work inspires further exploration and classification of new nonequilibrium universality classes beyond existing paradigms, paving the way for future discoveries in dynamical systems.

* shuoguang@uchicago.edu

† hanai.r.7e4b@m.isct.ac.jp

- [1] H. Hinrichsen, *Advances in Physics* **49**, 815 (2000).
- [2] M. Kardar, G. Parisi, and Y. C. Zhang, *Physical Review Letters* **56**, 889 (1986).
- [3] K. A. Takeuchi, *Physica A: Statistical Mechanics and its Applications* **504**, 77 (2018).
- [4] T. Vicsek, A. Czirak, E. Ben-Jacob, I. Cohen, and O. Shochet, *Physical Review Letters* **75**, 1226 (1995).
- [5] J. Toner and Y. Tu, *Physical Review Letters* **75**, 4326 (1995).
- [6] B. Mahault, F. Ginelli, and H. Chaté, *Phys. Rev. Lett.* **123**, 218001 (2019).
- [7] H. Ikeda, *Phys. Rev. Lett.* **133**, 258301 (2024).
- [8] H. Chaté and A. Solon, *Phys. Rev. Lett.* **132**, 268302 (2024).
- [9] A. N. Zaikin and A. M. Zhabotinsky, *Nature* **1970** 225:5232 **225**, 535 (1970).
- [10] S. H. Strogatz, *Nonlinear Dynamics And Chaos* (Westview, 2000).
- [11] A. T. Winfree, *The Geometry of Biological Time* (Springer, 2001).
- [12] V. Khemani, R. Moessner, and S. L. Sondhi, “A brief history of time crystals,” (2019), arXiv:1910.10745 [cond-mat.str-el].
- [13] R. Daviet, C. P. Zelle, A. Rosch, and S. Diehl, *Physical Review Letters* **132**, 167102 (2024).
- [14] R. Daviet, C. P. Zelle, A. Asadollahi, and S. Diehl, “Kardar-parisi-zhang scaling in time-crystalline matter,” (2024), arXiv:2412.09677 [cond-mat.stat-mech].
- [15] M. Fruchart, R. Hanai, P. B. Littlewood, and V. Vitelli, *Nature* **592**, 363 (2021).
- [16] Z. You, A. Baskaran, and M. C. Marchetti, *Proceedings of the National Academy of Sciences of the United States of America* **117**, 19767 (2020).
- [17] S. Saha, J. Agudo-Canalejo, and R. Golestanian, *Phys. Rev. X* **10**, 041009 (2020).
- [18] R. Hanai, A. Edelman, Y. Ohashi, and P. B. Littlewood, *Phys. Rev. Lett.* **122**, 185301 (2019).
- [19] R. Hanai and P. B. Littlewood, *Phys. Rev. Res.* **2**, 033018 (2020).
- [20] Y. Avni, M. Fruchart, D. Martin, D. Seara, and V. Vitelli, “Nonreciprocal ising model,” (2025), arXiv:2311.05471 [cond-mat.stat-mech].
- [21] Z.-F. Huang, M. te Vrugt, R. Wittkowski, and H. Löwen, “Active pattern formation emergent from single-species nonreciprocity,” (2024), arXiv:2404.10093 [cond-mat.soft].
- [22] F. Brauns and M. C. Marchetti, *Phys. Rev. X* **14**, 021014 (2024).
- [23] R. Hanai, *Phys. Rev. X* **14**, 011029 (2024).
- [24] G. Pisegna, S. Saha, and R. Golestanian, *Proceedings of the National Academy of Sciences* **121**, e2407705121 (2024).
- [25] E. I. R. Chiacchio, A. Nunnenkamp, and M. Brunelli, *Phys. Rev. Lett.* **131**, 113602 (2023).
- [26] S. A. M. Loos, S. H. L. Klapp, and T. Martynek, *Phys. Rev. Lett.* **130**, 198301 (2023).
- [27] T. Nadolny, C. Bruder, and M. Brunelli, *Phys. Rev. X* **15**, 011010 (2025).
- [28] C. P. Zelle, R. Daviet, A. Rosch, and S. Diehl, *Physical Review X* **14**, 021052 (2024).
- [29] C. Weis, M. Fruchart, R. Hanai, K. Kawagoe, P. B. Littlewood, and V. Vitelli, “Exceptional points in nonlinear and stochastic dynamics,” (2023), arXiv:2207.11667 [nlin.CD].
- [30] R. Belyansky, C. Weis, R. Hanai, P. B. Littlewood, and A. A. Clerk, “Phase transitions in nonreciprocal driven-dissipative condensates,” (2025), arXiv:2502.05267 [quant-ph].
- [31] D. Hardt, R. Doostani, S. Diehl, N. del Ser, and A. Rosch, “Propelling ferrimagnetic domain walls by dynamical frustration,” (2025), arXiv:2405.14320 [cond-mat.stat-mech].
- [32] R. Hanai, D. Ootsuki, and R. Tazai, “Photoinduced nonreciprocal magnetism,” (2024), arXiv:2406.05957 [cond-mat.str-el].
- [33] Y. Nakanishi, R. Hanai, and T. Sasamoto, “Continuous time crystals as a pt symmetric state and the emergence of critical exceptional points,” (2025), arXiv:2406.09018 [quant-ph].
- [34] T. Biancalani, F. Jafarpour, and N. Goldenfeld, *Phys.*

- Rev. Lett.* **118**, 018101 (2017).
- [35] T. Suchanek, K. Kroy, and S. A. M. Loos, *Phys. Rev. E* **108**, 064610 (2023).
- [36] T. Suchanek, K. Kroy, and S. A. M. Loos, *Phys. Rev. Lett.* **131**, 258302 (2023).
- [37] T. Suchanek, K. Kroy, and S. A. M. Loos, *Phys. Rev. E* **108**, 064123 (2023).
- [38] U. Alon, M. R. Evans, H. Hinrichsen, and D. Mukamel, *Phys. Rev. Lett.* **76**, 2746 (1996).
- [39] Q. Fontaine, D. Squizzato, F. Baboux, I. Amelio, A. Lemaître, M. Morassi, I. Sagnes, L. Le Gratiet, A. Harouri, M. Wouters, I. Carusotto, A. Amo, M. Richard, A. Minguzzi, L. Canet, S. Ravets, and J. Bloch, *Nature* **2022** 608:7924 **608**, 687 (2022).
- [40] A. Dinelli, J. O’Byrne, A. Curatolo, Y. Zhao, P. Sollich, and J. Tailleur, *Nature Communications* **14**, 7035 (2023).
- [41] J. Veenstra, O. Gamayun, X. Guo, A. Sarvi, C. V. Meinersen, and C. Coulais, *Nature* **627**, 528 (2024).
- [42] N. D. Mermin and H. Wagner, *Phys. Rev. Lett.* **17**, 1133 (1966).
- [43] L. He, L. M. Sieberer, E. Altman, and S. Diehl, *Physical Review B - Condensed Matter and Materials Physics* **92** (2015), 10.1103/PhysRevB.92.155307.

METHODS

Phase dynamics under stochastic noise

In this section, we review the critical fluctuation properties of our non-reciprocal $O(2)$ model in the vicinity of the CEP within the linearized theory [19]. We first rewrite Eq. (2) in the amplitude-phase representation and assume that the amplitude fluctuation is small and overdamped. This leads to the equation of motion that dominates the low-energy physics as,

$$\begin{aligned}\partial_t \theta_A &= -[a_A + b_A(\Delta\theta)^2]\Delta\theta + D_A \partial_x^2 \theta_A + \xi_A, \\ \partial_t \theta_B &= -[a_B + b_B(\Delta\theta)^2]\Delta\theta + D_B \partial_x^2 \theta_B + \xi_B.\end{aligned}\quad (7)$$

Here, we have omitted the higher-order nonlinearities that are irrelevant in the RG (renormalization group) sense. Notice that Eq. (7) are invariant under

$$\begin{aligned}\theta_a &\rightarrow \theta_a + \varphi, \text{ (where } \varphi \in \mathbb{R} \text{ is arbitrary)} \\ \theta_a &\rightarrow -\theta_a.\end{aligned}\quad (8)$$

$$(9)$$

as expected from the symmetry. We note that this symmetry excludes the KPZ-like terms such as $(\partial_x \theta_a)^2$.

Let us start with the linearized theory ($b_a = 0$) in the aligned phase ($a_A \geq a_B$)

$$\partial_t \theta_a = \hat{A}_{ab} \theta_b + \xi_a \quad (10)$$

with

$$\hat{A}_{ab} = \begin{pmatrix} -a_A + D_A \partial_x^2 & a_A \\ -a_B & a_B + D_B \partial_x^2 \end{pmatrix}_{ab}. \quad (11)$$

By Fourier transforming Eq. (10) and solving the secular equation $\det[-i\omega \mathbf{1} - \hat{A}(k)] = 0$, the eigenenergies are given by (up to $O(k^2)$)

$$\omega_{\pm}(k) = \frac{1}{2} \left[-i(\gamma + 2Dk^2) \pm \sqrt{-\gamma^2 + 4v^2 k^2} \right], \quad (12)$$

where $\gamma = a_A - a_B (\geq 0)$, $D = (D_A + D_B)/2$ and $v^2 = [(a_A + a_B)(D_B - D_A)]/2$. Here, $\gamma \geq 0$ characterizes the distance from the CEP.

When the system is away from the CEP ($\gamma > 0$), the eigenmodes are given by $\omega_+(k) \simeq -i\gamma$ and $\omega_-(k) \propto -ik^2$ for low momentum k , where the latter is the diffusive Goldstone mode. Since the former decays fast and therefore does not affect the asymptotic features, the diffusive Goldstone mode dominates the slow dynamics. In this case, there are no further nonlinearities that are non-irrelevant and therefore the system obeys the EW scaling, as demonstrated numerically in the main text.

At the CEP ($\gamma \rightarrow 0$), however, both eigenmodes $\omega_{\pm}(k)$ become gapless, which interestingly are sound modes

$$\omega_{\pm}(k) = \pm v|k| - iDk^2 \quad (13)$$

showing that both modes play a role and thus significantly modify the scaling properties.

To gain more insight, it is convenient to transform into the in-phase and out-of-phase basis ($s = \perp, \parallel$),

$$\begin{aligned}\delta \tilde{\theta}_s(k, \omega) &= \sum_a \mathcal{U}_{s,a} \delta \theta_a(k, \omega), \\ \tilde{\xi}_s(k, \omega) &= \sum_a \mathcal{U}_{s,a} \xi_a(k, \omega),\end{aligned}\quad (14)$$

with

$$\mathcal{U}^\dagger(k=0) = \frac{1}{\sqrt{2}} \begin{pmatrix} 1 & -1 \\ 1 & 1 \end{pmatrix}. \quad (15)$$

This transforms the kernel as

$$\tilde{A}(k) = \mathcal{U} A(k) \mathcal{U}^\dagger = \begin{pmatrix} -D_{\perp\perp} k^2 & \zeta - D_{\perp\parallel} k^2 \\ -D_{\parallel\perp} k^2 & -\gamma - D_{\parallel\parallel} k^2 \end{pmatrix}, \quad (16)$$

where $\zeta = a_A + a_B$, $D_{\perp\perp} = D_{\parallel\parallel} = (D_B + D_A)/2 = D$, and $D_{\perp\parallel} = D_{\parallel\perp} = (D_B - D_A)/2 = \frac{1}{\zeta} v^2$. Rewriting Eq. (10) in this new basis (in real space), we get

$$\begin{aligned}\partial_t \theta_{\perp} &= \zeta \theta_{\parallel} + D \partial_x^2 \theta_{\perp} + \frac{1}{\zeta} v^2 \partial_x^2 \theta_{\parallel} + \xi_{\perp}, \\ \partial_t \theta_{\parallel} &= -\gamma \theta_{\parallel} + D \partial_x^2 \theta_{\parallel} + \frac{1}{\zeta} v^2 \partial_x^2 \theta_{\perp} + \xi_{\parallel}\end{aligned}\quad (17)$$

One immediate observation is that nonreciprocity is preserved in Eq. (17) in terms of one-way coupling, where θ_{\parallel} drives the dynamics of θ_{\perp} , but not the other way around in the global limit $\partial_x \theta_{\perp}, \partial_x \theta_{\parallel} \rightarrow 0$. As a result of this one-way coupling, the eigenmodes are generically not orthogonal. In particular, one finds that the two eigenmodes are given by

$$\begin{pmatrix} \theta_{\perp} \\ \theta_{\parallel} \end{pmatrix} \propto \begin{pmatrix} 1 \\ 0 \end{pmatrix}, \quad \begin{pmatrix} \theta_{\perp} \\ \theta_{\parallel} \end{pmatrix} \propto \begin{pmatrix} 1 + \frac{a_A}{a_B} \\ 1 - \frac{a_A}{a_B} \end{pmatrix}, \quad (18)$$

in the $k \rightarrow 0$ limit, which has eigenenergies $\omega_-(k=0) = 0$, $\omega_+(k=0) = -i\gamma$, respectively. As one sees, the Goldstone mode $\omega_-(k=0)$ is associated with the center of mass phase $\Theta = (\theta_A + \theta_B)/2 (= \theta_{\perp}/\sqrt{2})$. The other mode, which becomes gapless at the CEP $\gamma = a_A - a_B = 0$, importantly *coalesces* with the Goldstone mode. As will be seen soon later, this unique property gives rise to anomalously giant fluctuations at the CEP.

Anomalously Giant Phase Fluctuations At CEP

The above peculiar property (i.e. coalescence of two gapless sound modes) at the CEP gives rise to anomalously giant phase fluctuations. To see this in a transparent way, let us investigate the behavior of the equal-time correlation function $\langle \theta_a(\mathbf{r}) \theta_b(\mathbf{r}') \rangle$.

First, let us calculate the Green's function by Fourier transforming Eq. (17)

$$-i\omega\tilde{\theta}_s = \tilde{A}_{ss'}\tilde{\theta}_s + \tilde{\xi}_s \Rightarrow \tilde{\theta}_s = G_{ss'}^0\xi_{s'} \quad (19)$$

where in this basis, $\tilde{G}_{ss'}^0(k, \omega) = [-i\omega\mathbf{1} - \tilde{A}(k, \omega)]_{ss'}^{-1}$ is given by (put $\gamma = 0$)

$$\begin{aligned} & \tilde{G}^0(k, \omega) \\ &= \frac{1}{[\omega - \omega_-(k)][\omega - \omega_+(k)]} \begin{pmatrix} i\omega - Dk^2 & -\zeta + \frac{v^2}{\zeta}k^2 \\ \frac{v^2}{\zeta}k^2 & i\omega - Dk \end{pmatrix}. \end{aligned} \quad (20)$$

In the equal-time correlation $\langle \theta_\alpha(-k, -\omega)\theta_\beta(k, \omega) \rangle = \langle \tilde{G}_{\alpha s'}^0(-k, -\omega)\xi_{s'}(-k, -\omega)\xi_s(k, \omega)\tilde{G}_{s\beta}^0(k, \omega) \rangle$, by counting the order of poles, we realize $\tilde{G}_{\perp\parallel}$ exhibits the strongest singularity at the CEP. As a result, the term that involves two $\tilde{G}_{\perp\parallel}$ gives the most dominant effect to the two correlation function, leading to,

$$\begin{aligned} \langle \theta_a(\mathbf{r})\theta_b(\mathbf{r}') \rangle &\sim \int_0^{\Lambda_c} dk k^{d-1} e^{ik\cdot(\mathbf{r}-\mathbf{r}')} \\ &\times \int_{-\infty}^{\infty} \frac{d\omega}{2\pi} \tilde{G}_{\perp\parallel}^0(k, \omega)\sigma_{\parallel\parallel}\tilde{G}_{\perp\parallel}^0(-k, -\omega) \\ &\sim \int_0^{\Lambda_c} dk k^{d-1} e^{ik\cdot(\mathbf{r}-\mathbf{r}')} \cdot \frac{B}{k^4}, \end{aligned} \quad (21)$$

with $B = \zeta^2\sigma_{\parallel\parallel}/(v^2D)$ which diverges at $d \leq 4$. The phase fluctuations are anomalously giant, in the sense that it is large compared to the equilibrium counterpart, $\langle \theta^2 \rangle \sim \int_0^{\Lambda_c} dk k^{d-1} \cdot k^{-2}$, which diverges only for $d \leq 2$, as stated in the Mermin-Wagner-Hohenberg Theorem [42]. As is clearly in this structure, the giant fluctuations are activated by the noise $\sigma_{\parallel\parallel}$ gets converted to the Goldstone mode through the nonreciprocal mixing ζ .

Linear Theory of CEP Scaling

Assume a universal dynamical scaling near CEP such as,

$$\langle \theta_a(\mathbf{r}, t)\theta_b(\mathbf{r}', t') \rangle = |\mathbf{r} - \mathbf{r}'|^{2\alpha} \mathcal{F}_{ab}\left(\frac{t-t'}{|\mathbf{r} - \mathbf{r}'|^z}\right), \quad (22)$$

where $\mathcal{F}_{ab}(x)$ is a scaling function. α is the roughness exponent, and z is dynamical exponent. To find the fixed

points and thereby the critical exponents, consider the rescaling of space, time and phase fluctuations according to

$$\mathbf{r} \rightarrow e^l \mathbf{r}, t \rightarrow e^{z l} t, \theta_a \rightarrow e^{\alpha l} \theta_a. \quad (23)$$

By simple power counting, the rescaling of the parameters in Eq. (17) follows

$$\zeta \rightarrow e^{z l} \zeta, \gamma \rightarrow e^{z l} \gamma, v \rightarrow e^{(z-1)l} v, \quad (24)$$

$$D \rightarrow e^{(z-2)l} D, \sigma_{ss'} \rightarrow e^{(z-d-2\alpha)l} \sigma_{ss'}. \quad (25)$$

We demand that the parameter B , which gives the magnitude of the equal time correlation function, to be fixed at the Gaussian fixed point. This can be obtained from the flow equation of B ,

$$\begin{aligned} \frac{dB}{dl} &= \left(\frac{2}{\zeta} \frac{d\zeta}{dl} + \frac{1}{\sigma_{\parallel\parallel}} \frac{d\sigma_{\parallel\parallel}}{dl} - \frac{1}{D} \frac{dD}{dl} - \frac{2}{v} \frac{dv}{dl} \right) B \\ &= (4 - d - 2\alpha)B, \end{aligned} \quad (26)$$

which yields the roughening exponent $\alpha_{\text{Gauss}} = (4-d)/2$ at CEP. Especially when $d = 1$, we find $\alpha_{\text{Gauss}} = 3/2$.

Simulation Method

We use the Euler-Maruyama method to numerically solve the full non-reciprocal $O(2)$ model (Eq. (2)), applying spatial periodic boundary conditions are applied in all simulations. For the CEP scaling simulations (Fig. 2 and 3), we initialize the system in uniform steady states at each j_+ to prevent the formation of topological defects during long-time evolution. For dynamical pattern formation simulations (Fig. 4(b-c) and 5), we use random initial conditions to rapidly activate pattern formation. Unless otherwise specified, ensemble averages are performed over 96 stochastic trials.

To calculate the equal-time correlation $w_a(t, L)$, we first extract the phase modes from \vec{P}_a , and then unwind the phase by ensuring that the phase difference between adjacent time steps remain less than π (i.e. no 2π phase jump as in the compact phase) [43].